Probing the Cruzain S_2 Recognition Subsite: A Kinetic and Binding Energy Calculation Study†

Fabio Polticelli,*,‡ Germano Zaini,‡ Alessandro Bolli,‡ Giovanni Antonini,‡ Luigi Gradoni,§ and Paolo Ascenzi‡,||

Dipartimento di Biologia and Laboratorio Interdipartimentale per la Microscopia Elettronica, Viale Guglielmo Marconi 446, I-00146 Roma, Italy, Laboratorio di Parassitologia, Istituto Superiore di Sanità, Viale Regina Elena 299, I-00161 Rome, Italy, and Istituto Nazionale per le Malattie Infettive I.R.C.C.S. "Lazzaro Spallanzani", Via Portuense 292, I-00149 Roma, Italy

Received July 26, 2004; Revised Manuscript Received December 20, 2004

ABSTRACT: Cysteine proteases are relevant to several aspects of the parasite life cycle and the parasite−host relationship. Moreover, they appear as promising targets for antiparasite chemotherapy. Here, a quantitative investigation on the catalytic properties of cruzain, the papain-like cysteine protease from epimastigotes of *Trypanosoma cruzi*, is reported. The results indicate that kinetics for the cruzain catalyzed hydrolysis of *N*-α-benzyloxycarbonyl-L-arginyl-L-alanine-(7-amino-4-methylcoumarin), *N*-α-benzyloxycarbonyl-L-phenylalanyl-L-alanine-(7-amino-4-methylcoumarin), and *N*-α-benzyloxycarbonyl-L-tyrosyl-L-alanine-(7-amino-4-methylcoumarin) can be consistently fitted to the minimum three-step mechanism of cysteine proteases involving the acyl·enzyme intermediate E·P; the deacylation step is rate-limiting in enzyme catalysis. Remarkably, these substrates show identical catalytic parameters. This reflects the ability of the cruzain Glu205 residue, located at the bottom of the S_2 subsite, to neutralize the substrate/inhibitor polar P_2 residues (e.g., Arg or Tyr) and to be solvent-exposed when substrate/inhibitor nonpolar P_2 residues (e.g., Phe) fit the S_2 subsite. More complex catalytic mechanisms are also discussed. Binding free-energy calculation provides a quantitative framework for the interpretation of these results; in particular, direct evidence for the compensatory effect between Coulomb interaction(s) and solvation effect(s) is reported. These results appear of general significance for a deeper understanding of (macro)molecular recognition and for the rational design of novel inhibitors of parasitic cysteine proteases.

Trypanosomatids are parasitic protozoa, a number of them being agents of endemic diseases prevalent mainly in developing countries. In particular, *Trypanosoma cruzi* is the agent of Chagas' disease, affecting at least 20 million people. Remarkably, a much larger population is considered at risk of trypanosomiasis, a major public health problem being the transmission of this parasitic disease through blood transfusion and organ transplantation (*1*).

Cysteine proteases appear to be relevant to several aspects of the *T. cruzi* life cycle and the parasite−host relationship. In particular, cruzain, the major cysteine protease from *T. cruzi* epimastigotes, is expressed in all stages of the parasite life cycle, being more abundant in replicating forms and particularly in the insect epimastigote stage. Notably, cruzain participates in the penetration of *T. cruzi* trypomastigotes into host cells, in the nutrition of the parasite at the expense of the host, and in the escape mechanisms of the parasite from the immune system of the host. Therefore, cruzain has been regarded as a promising target for antiparasite chemotherapy. In fact, cysteine protease inhibitors block replication and differentiation of *T. cruzi* both *in vitro* and *in vivo*, providing an alternative to traditional therapy in drug-resistant parasites (*2*−*9*).

Most proteases display a well-defined specificity for a restricted set of chemically homogeneous substrates and inhibitors. A well-known example is represented by trypsin-like enzymes, which catalyze the hydrolysis of substrates displaying basic residues at position P_1 (*10*−*13*). This specificity is achieved by the binding of the substrate or the inhibitor P_1 residue to the solvent-screened S_1 pocket on the bottom of which is located the acidic residue Asp189. In this respect, cruzain is peculiar in that this enzyme, as well as cathepsin B and related cysteine proteases, has evolved a dual specificity that allows tight binding and catalysis on both basic and aromatic residues (*14*). In cathepsin-B-like proteases, binding of the substrate or inhibitor P_2 residue to the enzyme-shallow S_2 specificity subsite, lined by hydrophobic residues and faced by a solvent-accessible Glu residue (Glu205 in cruzain), is the major determinant for substrate and inhibitor selection. In contrast, the chemical nature of substrate or inhibitor P_1 and P_3 residues is less relevant (*14*−*16*). The low selectivity of cruzain is essentially due to the hydrophobic nature of the S_2 pocket and to the flexibility of Glu205, which can adopt different conformations depending on the nature of the substrate or inhibitor bound. In particular, Glu205 is solvent-exposed when nonpolar residues are bound in the S_2 specificity subsite, whereas it is oriented toward the substrate when basic residues are bound (Figure 1) (*14*).

† This study was partly supported by grants from the Ministry of Education, University, and Research of Italy (MIUR, FIRB-2001 to F.P., L.G., and P.A.).

* To whom correspondence should be addressed. Telephone: +39-06-5517-6362. Fax: +39-06-5517-6321. E-mail: polticel@uniroma3.it.

‡ Università "Roma Tre".

§ Istituto Superiore di Sanità.

|| Istituto Nazionale per le Malattie Infettive I.R.C.C.S. "Lazzaro Spallanzani".

10.1021/bi048417v CCC: $30.25
Published on Web 02/05/2005

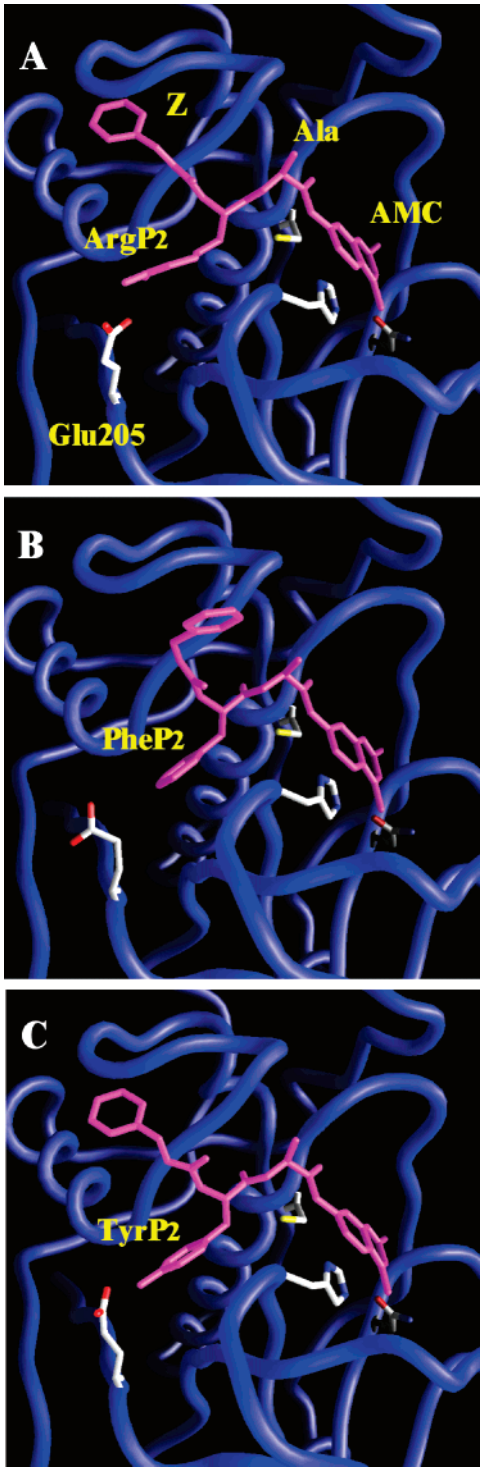

FIGURE 1: Schematic representation of the three-dimensional models of the noncovalent complexes formed by cruzain with Z-Arg-Ala-AMC (A), Z-Phe-Ala-AMC (B), and Z-Tyr-Ala-AMC (C). The substrates, the catalytic triad residues (Cys25, His159, and Asn175), and Glu205 are depicted in stick representation. For clarity, only the A conformations (see the Materials and Methods) of the cruzain:Z-Arg-Ala-AMC and cruzain:Z-Tyr-Ala-AMC complexes are shown. Note the substrate-directed conformation of Glu205 in the cruzain:Z-Arg-Ala-AMC and cruzain:Z-Tyr-Ala-AMC complexes and the solvent-oriented conformation of Glu205 in the cruzain:Z-Phe-Ala-AMC complex. The figure was made with Grasp (*34*).

Interestingly, papain-like cysteine proteases, which display a Ser residue at position 205, are characterized by a 100-fold higher Phe versus Arg selectivity as compared to cruzain (*9*, *17*−*20*).

The present study reports a quantitative investigation on the kinetics of the cruzain-catalyzed hydrolysis of fluorogenic substrates *N*-α-benzyloxycarbonyl-L-arginyl-L-alanine-(7-amino-4-methylcoumarin) (Z-Arg-Ala-AMC),[1] *N*-α-benzyloxycarbonyl-L-phenylalanyl-L-alanine-(7-amino-4-methylcoumarin) (Z-Phe-Ala-AMC), and *N*-α-benzyloxycarbonyl-L-tyrosyl-L-alanine-(7-amino-4-methylcoumarin) (Z-Tyr-Ala-AMC). The catalytic parameters for the enzymatic hydrolysis of the three substrates are identical. Binding energy calculations provide evidence for a compensatory effect between Coulombic interaction(s) and solvation effect(s), such that, when a basic substrate binds to the cruzain S_2 recognition subsite, charge−charge interactions make a favorable contribution to binding, but the energy penalty for desolvation of the interacting partners yields an overall destabilizing electrostatic energy. However, when aromatic substrates bind to the cruzain S_2 recognition subsite, Coulombic interactions are much less stabilizing but the increased solvent accessibility of Glu205 lowers the desolvation penalty and the calculated electrostatic energy is similar to that obtained for the basic substrate. The relevance of these results in the understanding of macromolecular recognition processes is discussed.

MATERIALS AND METHODS

Enzyme. Cruzain was prepared from *T. cruzi* (CAN-III strain) epimastigotes. The reducing agent dithiothreitol does not significantly activate (<10%) the freshly prepared cruzain. The concentration of active cruzain was determined by active-site titration with L-*trans*-epoxysuccinylleucylamido(4-guanidino)butane (*21*).

Chemicals. Z-Arg-Ala-AMC, Z-Phe-Ala-AMC, and Z-Tyr-Ala-AMC were purchased from Enzyme System Products (Livermore, CA). Dithiothreitol and L-*trans*-epoxysuccinylleucylamido(4-guanidino)butane were obtained from Sigma−Aldrich (St. Louis, MO). All of the other products were obtained from Merck AG (Darmstadt, Germany). All chemicals were of analytical grade and were used without further purification.

Cysteine Protease Assay. The hydrolysis of the fluorogenic substrates Z-Arg-Ala-AMC, Z-Phe-Ala-AMC, and Z-Tyr-Ala-AMC catalyzed by cruzain was monitored in continuous assays. Briefly, Z-Arg-Ala-AMC, Z-Phe-Ala-AMC, or Z-Tyr-Ala-AMC (final concentration of 5.0×10^{-7} to 4.0×10^{-5} M) was mixed with the cruzain solution (final concentration of 1.0×10^{-7} to 4.0×10^{-5} M), and fluorescence (380 nm excitation wavelength and 460 nm absorption wavelength) was measured, at pH 6.5 (phosphate buffer, $I = 0.1$ M) and 37.0 °C. The amount of Z-Arg-Ala-AMC, Z-Phe-Ala-AMC, and Z-Tyr-Ala-AMC hydrolyzed by cruzain (i.e., of AMC released) was calibrated letting the enzymatic

[1] Abbreviations: AMC, 7-amino-4-methylcoumarin; Z-Arg-Ala-AMC, *N*-α-benzyloxycarbonyl-L-arginyl-L-alanine-(7-amino-4-methylcoumarin); Z-Arg-Ala-FMK, *N*-α-benzyloxycarbonyl-L-arginyl-L-alanine fluoromethyl-ketone; Z-Phe-Ala-AMC, *N*-α-benzyloxycarbonyl-L-phenylalanyl-L-alanine-(7-amino-4-methylcoumarin); Z-Phe-Ala-FMK, *N*-α-benzyloxycarbonyl-L-phenylalanyl-L-alanine fluoromethyl-ketone; Z-Tyr-Ala-AMC, *N*-α-benzyloxycarbonyl-L-tyrosyl-L-alanine-(7-amino-4-methylcoumarin); Z-Tyr-Ala-FMK, *N*-α-benzyloxycarbonyl-L-tyrosyl-L-alanine fluoromethyl-ketone.

Scheme 1

$$\begin{array}{ccccccc} & & K_s & & k_{+2} & & k_{+3} \\ E + S & \leftrightarrow & E{:}S & \rightarrow & E{\cdot}P & \rightarrow & E + P2 \\ & & & & + & & \\ & & & & P1 & & \end{array}$$

reaction go to completion and measuring the total amplitude of the signal (*21*).

Determination of Catalytic Parameters. Kinetics of the cruzain-catalyzed hydrolysis of Z-Arg-Ala-AMC, Z-Phe-Ala-AMC, and Z-Tyr-Ala-AMC was analyzed in the framework of the minimum three-step mechanism (Scheme 1) (*9*, *21*−*24*). E is the enzyme; S is the substrate; E:S is the reversible rapidly formed enzyme/substrate complex; E·P is the acyl· intermediate; P1 is the fluorogenic (i.e., AMC) hydrolysis product; P2 is the nonfluorogenic (i.e., Z-Arg-Ala, Z-Phe-Ala, or Z-Tyr-Ala) hydrolysis product; K_s is the dissociation equilibrium constant for the formation of the reversible E:S complex; k_{+2} is the first-order acylation rate constant; k_{+3} is the first-order deacylation rate constant; K_m ($=k_{+3}K_s/(k_{+2} + k_{+3})$) is the Michaelis constant; and k_{cat} ($=k_{+2}k_{+3}/(k_{+2} + k_{+3}) = V_{max}/[E]$, where V_{max} and [E] represent the maximum velocity at [S] > $10K_m$ and the active enzyme concentration, respectively), is the catalytic constant. More complex catalytic mechanisms cannot be ruled out. Among others, we cannot exclude that the rate-limiting step may be represented by a conformational change(s) following product P_2 dissociation and preceding the recovery of the active E species, ready for the next catalytic cycle, instead of the deacylation step. However, this reaction pathway is kinetically indistinguishable from the simple three-step mechanism (Scheme 1).

Values of K_m, k_{cat}, and k_{cat}/K_m were determined from plots of the initial rate for substrate hydrolysis (i.e., v_i) versus [S], with [S] ≥ 5[E], according to the Michaelis eq 1 (*9*, *21*−*24*)

$$v_i = k_{cat} \times [S]/(K_m + [S]) \quad (1)$$

When [S] ≥ 5[E], the differential equations arising from Scheme 1 may be solved to describe the time course of P1 release (eqs 2−5) (*9*, *21*−*24*).

$$[P_1] = k_{cat}[E]t/\{1 + K_m/[S]\} + \alpha[E](1 - e^{-lt}) \quad (2)$$

where

$$\pi = \alpha[E] \quad (3)$$

corresponds to the total amplitude of the burst phase of P1 release

$$\alpha = \{k_{+2}/(k_{+2} + k_{+3})/(1 + K_m/[S])\}^2 \quad (4)$$

is the molar fraction of the substrate-bound enzyme, and

$$l = \{k_{+2}[S]/(K_s + [S])\} + k_{+3} \quad (5)$$

is the first-order rate constant for the burst phase of P1 release. According to eqs 2−5, when $k_{+2} \geq k_{+3}$, a burst of P1 release of amplitude π with a first-order rate constant l is experimentally detectable. Therefore, values of K_m, K_s, k_{+2}, k_{+2}/K_s, and k_{+3} were determined from plots of $\sqrt{\alpha}$ versus [S] and l versus [S], with [S] ≥ 5[E] and $k_{+2} \geq k_{+3}$, according to eqs 4 and 5.

Values of K_s, k_{+2}, and k_{+2}/K_s were determined from the dependence of the first-order rate constant for the formation of the E:P complex (i.e., k) on the enzyme concentration, with [E] ≥ 5[S], according to eq 6 (*9*, *21*−*24*)

$$k = k_{+2}[E]/(K_s + [E]) \quad (6)$$

Values of k_{+3} were calculated from values of K_m, k_{cat}, K_s, and k_{+2} according to eqs 7 and 8 (*9*, *21*−*24*)

$$k_{+3} = k_{cat}k_{+2}/(k_{+2} - k_{cat}) \quad (7)$$

$$k_{+3} = k_{+2}K_m/(K_s - K_m) \quad (8)$$

A statistical analysis was performed using Student's *t* test with the INSTAT software system for Windows. In all cases, probability (p) values below 0.005 were considered significant.

Best fit of the experimental data to Scheme 1 was performed using GEPASI 3.30 (*25*−*27*). The program carries out the nonlinear minimization of the kinetic constants by means of numerical integration at variable steps of the ordinary differential equations.

Molecular Structures. Molecular models of the noncovalent complexes formed by cruzain with Z-Arg-Ala-AMC, Z-Tyr-Ala-AMC, and Z-Phe-Ala-AMC (i.e., E:S in Scheme 1) were derived from the crystal structures of the covalent adducts formed by reaction of cruzain with *N*-α-benzyloxycarbonyl-L-arginyl-L-alanine fluoromethyl-ketone (Z-Arg-Ala-FMK) (PDB code 2AIM) (*14*), *N*-α-benzyloxycarbonyl-L-tyrosyl-L-alanine fluoromethyl-ketone (Z-Tyr-Ala-FMK) (PDB code 1AIM) (*14*), and *N*-α-benzyloxycarbonyl-L-phenylalanyl-L-alanine fluoromethyl-ketone (Z-Phe-Ala-FMK) (*15*) (i.e., E·P in Scheme 1). These inhibitors bind covalently to cruzain at Cys25 with the concurrent release of fluoride. In the cruzain·Z-Arg-Ala-FMK complex, two different conformations with approximately 40 and 60% occupancy were observed for the Arg P_2 residue (*14*). In the high-occupancy conformation (conformation A), thought to be the more physiologically relevant, the Arg P_2 side chain forms a salt bridge, characterized by good geometry and distances, with Glu205. The low-occupancy conformation (conformation B) is a crystal-packing artifact in that the guanidinium group of the Arg P_2 side chain is rotated out of the S_2 pocket and forms a salt bridge with the C terminus of another cruzain molecule in the unit cell. In the cruzain·Z-Tyr-Ala-FMK complex, two different conformations for Glu205 were modeled in the final electron-density map (*14*). In the high-occupancy (70%) conformation (conformation A), Glu205 side chain is positioned such as to interact with the TyrP_2 hydroxyl group. In the low-occupancy (30%) conformation (conformation B), Glu205 is rotated away from the inhibitor and fully solvent-exposed.

The coordinates of cruzain:Z-Arg-Ala-AMC, cruzain:Z-Tyr-Ala-AMC, and cruzain:Z-Phe-Ala-AMC noncovalent complexes (i.e., E:S in Scheme 1) were obtained by breaking the covalent bond between the cruzain Cys25 residue and Z-Arg-Ala-MK, Z-Tyr-Ala-MK, and Z-Phe-Ala-MK and adding the AMC group to the substrate carbonyl carbon using the Biopolymer module of InsightII (Molecular Simulations

Inc., San Diego, CA). The geometry of the AMC group relative to the *N*-α-benzyloxycarbonyl-aminoacyl-Ala moiety was modeled so as to avoid steric clashes with cruzain side chains. The model-built structures were stereochemically regularized as previously described (*12*). Briefly, the modeled complexes were first energy-minimized and then subjected to a 60 ps molecular dynamics simulation run in explicit solvent using CHARMM (*28*) and the CHARMM22 parameters and force field (*29*). Equilibrium, as judged by convergence of the root-mean-square deviation (rmsd) of non-hydrogen atoms positioned from the initial structures (Δrmsd < 0.05 Å) was reached in all complexes after approximately 40 ps.

Note that the model of the cruzain:Z-Phe-Ala-AMC complex (Figure 1) is in good agreement with the X-ray structure of two noncovalent complexes formed by cruzain with hydroxymethyl ketone inhibitors displaying a Phe residue at position P_2 (*30*). The rmsd value calculated on the Phe P_2 atoms is in both cases lower than 0.5 Å (data not shown). However, the complexes formed by cruzain with hydroxymethyl ketone reversible inhibitors do not yield covalent adducts (i.e., E·P; see Scheme 1) because of the unfavorable geometry for the attack of the thiol group of the catalytic Cys25 residue to the electron acceptor ketone C atom (*30*). Thus, we cannot exclude that in solution the occupancy of the S_2 specificity subsite by the P_2 residue of the Z-aminoacyl-aminoacyl-AMC substrates is lower than that observed in the crystals of cruzain−inhibitor covalent and reversible complexes (*14*, *30*).

Binding Free-Energy Calculations. Binding energy calculations were carried out on both conformers of the cruzain:Z-Arg-Ala-AMC and cruzain:Z-Tyr-Ala-AMC complexes (see above). However, it must be kept in mind that the B conformation of the cruzain:Z-Arg-Ala-AMC complex (40% occupancy) is a crystal-packing artifact and that the occupancy of the B conformation of the cruzain:Z-Tyr-Ala-AMC is only about 30% (*14*). Thus, values obtained on the A conformers of both the cruzain:Z-Arg-Ala-AMC and cruzain-Z:Tyr-Ala-AMC complexes (Figure 1) are the most appropriate to compare experimental and calculated binding energy values.

The method used here for the calculation of the total binding free energy ΔG_b for protein/ligand interaction is based on the energy decomposition proposed by Froloff and co-workers (*31*). Then, ΔG_b can be written according to eq 9

$$\Delta G_b = \Delta G_{el} + \Delta G_{np} + \Delta G_{strain} - T\Delta S_{sc} - T\Delta S_l - T\Delta S_{t,r} \quad (9)$$

where ΔG_{el} is the electrostatic contribution to binding, ΔG_{np} is the contribution because of nonpolar interactions between the protein and the ligand, ΔG_{strain} is a term that includes possible distortions of the protein and substrate upon complex formation, $T\Delta S_{sc}$ is the loss of conformational entropy of the protein side chain(s) upon ligand binding, $T\Delta S_l$ is the corresponding term for the ligand, and $T\Delta S_{t,r}$ describes the loss of translational and rotational degrees of freedom.

ΔG_{el} was calculated as the sum of the Coulomb and solvation energies of the complex *minus* those of the isolated species according to eq 10 (*32*, *33*)

$$\Delta G_{el}(\epsilon_i,\epsilon_o) = \Delta G_{coul}(\epsilon_i) + \Delta G_{solv}(\epsilon_i,\epsilon_o) \quad (10)$$

where $\Delta G_{el}(\epsilon_i,\epsilon_o)$ is the change in electrostatic free energy for the two reactants with interior dielectric constant ϵ_i in a medium of dielectric constant ϵ_o, $\Delta G_{coul}(\epsilon_i)$ is the Coulombic interaction between the two species in a medium of dielectric constant ϵ_i, and $\Delta G_{solv}(\epsilon_i,\epsilon_o)$ is the change in solvation energy upon transfer of the reactants from a medium of dielectric constant ϵ_i to a medium of dielectric constant ϵ_o.

Electrostatic potentials were calculated using DelPhi (*34*), which solves the finite difference Poisson−Boltzmann equation for molecules of complex shape by mapping the dielectric and charge distribution of the molecules in a three-dimensional grid. Atomic charges and radii were taken from the PARSE parameter set (*35*), and values of 2 and 80 were chosen for the dielectric constant of the molecules and solvent, respectively. The grid resolution was set to 3 grid units/Å. Each ΔG_{sol} value is the average of seven different calculations in which the molecules were translated in the grid by ±1.0 Å increments along the three axes. In each case, the deviation of ΔG_{sol} was less than ±0.1 kcal/mol.

The nonpolar contribution to binding was calculated according to eq 11 (*31*)

$$\Delta G_{np} = \gamma_{aw} A_c \quad (11)$$

where γ_{aw} is the microscopic surface tension associated with the transfer of an alkane from liquid alkane to water and A_c is the curvature-corrected accessible area lost by the two interacting partners upon complexation. Correction of the accessible area for curvature is needed to take into account the increase in hydrophobicity of the concave regions of the protein surface (*34*, *36*). γ_{aw} was set at 58.18 cal/Å^2 (*12*, *31*), and A_c was calculated using SURFCV (*37*).

Conformational entropy loss of the nonpeptidic portions of the substrates upon binding to cruzain was calculated according to eq 12 (*38*)

$$-T\Delta S = \sum RT \ln(N_{free}/N_{bound}) \quad (12)$$

where N_{free} is the number of torsion angles available in the unbound state and N_{bound} is the corresponding number in the bound state. As more than 60% of the total surface area of the substrates becomes buried upon binding to cruzain (data not shown), their conformation was considered fixed in the bound state. Thus, three configurations per rotatable bond were assumed in the free state and only one, in the bound state (*38*).

Conformational entropy loss for the protein side chains and for the peptidic portions of the substrates was obtained from the entropy scale of Pickett and Sternberg (*39*), developed assuming that side chains that are less than 40% buried rotate freely, while side chains that are more than 40% buried are restricted to one rotamer (*39*). Percentage of buried area was calculated with SURFCV (*37*) as the ratio between the accessible area of the amino acid side chain in the extended state and in the protein. ΔG_{strain} and $T\Delta S_{t,r}$ cannot be calculated directly and thus are a major source of error in the calculations. However, their contribution is expected to be very similar for all complexes. Thus, the error should affect mainly absolute binding energy values while still allowing a careful comparison of the other energetic

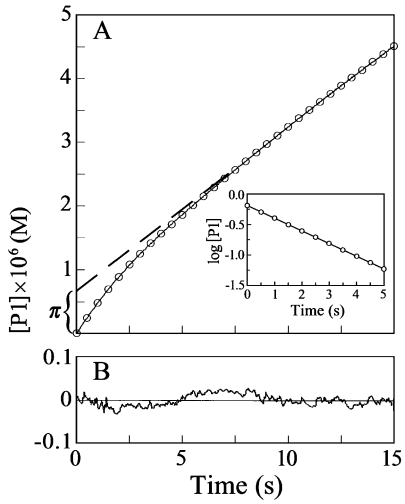

FIGURE 2: Time-course of the burst phase of AMC release during the cruzain-catalyzed hydrolysis of Z-Arg-Ala-AMC (A). The dashed line was extrapolated from the steady-state phase of AMC release after more than five half-times of the burst phase. The total amplitude of the burst phase of AMC release (i.e., π) corresponds to 0.65×10^{-6} M cruzain. The experimentally determined value of α (=0.33; inset) is in excellent agreement with that calculated according to eq 4 ($\alpha = 0.32$). The time course of the burst phase conforms to a single-exponential decay for more than 90% of its course (○ indicate experimental data). The experimentally determined value of l (=0.48 s^{-1}; inset) corresponds to that calculated according to eq 5 ($l = 0.48$ s^{-1}). The continuous line represents the best fit of the experimental data carried out by nonlinear minimization of the kinetic constants by means of numerical integration at variable steps of the ordinary differential equations. The following parameters were found: $k_{+1} \geq 1 \times 10^7$ M^{-1} s^{-1}, $k_{-1} \geq 80$ s^{-1}, K_s ($=k_{-1}/k_{+1}$) $= (8 \pm 4) \times 10^{-6}$ M, $k_{+2} = 0.5 \pm 0.05$ s^{-1}, and $k_{+3} = 0.2 \pm 0.03$ s^{-1}. Residual error plot (experimental *minus* simulated data) from the nonlinear minimization procedure (B). All data were obtained at pH 6.5 and 37.0 °C, with [S] $= 1.0 \times 10^{-5}$ M and [E] $= 2.0 \times 10^{-6}$ M. For further details, see the text.

terms, which determine substrate binding to cruzain in relative terms (for further details, see ref *12*).

RESULTS AND DISCUSSION

Kinetic Analysis for Cruzain Action. When [S] ≥ 5[E], the cruzain-catalyzed hydrolysis of Z-Arg-Ala-AMC, Z-Phe-Ala-AMC, and Z-Tyr-Ala-AMC shows, in the early stages of the reaction, an instantaneous release of AMC (i.e., P1; see Scheme 1) preceding the steady-state reaction (burst phase) (Figure 2).

The analysis (according to eq 1) of the steady-state reaction (i.e., v_i versus [S]) allows determination of K_m, k_{cat}, and k_{cat}/K_m values (Figure 3 and Table 1). Under all of the experimental conditions, the fluorescence change (i.e., the AMC formation) is linear over the assay time (3 min) (Figure 2), the dependence of the initial velocity (i.e., v_i) on the substrate concentration follows simple saturation kinetics (Figure 3), and v_i is a linear function of the cruzain concentration at fixed [S] (data not shown).

The analysis (according to eqs 4 and 5) of the burst phase of AMC release (i.e., $\sqrt{\alpha}$ versus [S] and l versus [S]) allows determination of K_m, K_s, k_{+2}, k_{+2}/K_s, and k_{+3} values (Figure 3 and Table 1). Under all of the experimental conditions, the value of the total amplitude of the burst phase (i.e., π) obtained experimentally is in agreement with that calculated according to eq 3 (Figures 2 and 3). The time course of the burst phase conforms to a single-exponential decay for more than 90% of its course (Figure 2), and the dependence of the molar fraction of the substrate-bound enzyme (i.e., $\sqrt{\alpha}$) and of the first-order rate constant for the burst phase of AMC release (i.e., l) on the substrate concentration follows simple saturation kinetics (Figure 3). According to eq 3, π is a linear function of the cruzain concentration at fixed [S] (data not shown).

Under all of the experimental conditions, no lag phase is detectable in AMC release after mixing E with S ([E] ≥ 5[S]), indicating that the process of E:S formation from E and S is complete within 2 ms, the dead time of the rapid-mixing stopped-flow apparatus. Such a finding is consistent with the following values of rate constants obtained from the nonlinear fitting procedure: k_{+1} ($=k_{-1}/K_s$) $\geq 10 \times 10^6$ M^{-1} s^{-1} and $k_{-1} \geq 80$ s^{-1} (Figure 2). This agrees with the classical assumption $k_{-1} \gg k_{+2}$ (*21*−*24*).

The analysis (according to eq 6) of the pre-steady-state reaction (i.e., k versus [E]) allows determination of K_s, k_{+2}, and k_{+2}/K_s values (Figure 3 and Table 1). Under all of the experimental conditions, the time course of the pre-steady-state reaction conforms to a single-exponential decay for more than 90% of its course and the dependence of the first-order rate constant for the pre-steady-state reaction (i.e., k) on the enzyme concentration follows simple saturation kinetics (Figure 3).

Kinetics for the cruzain-catalyzed hydrolysis of Z-Arg-Ala-AMC, Z-Phe-Ala-AMC, and Z-Tyr-Ala-AMC consistently fit the minimum three-step mechanism (Scheme 1) of cysteine proteases (*9*, *21*−*24*), as demonstrated from the almost identical values of kinetic parameters obtained under very different conditions (see Figures 2 and 3 and Table 1).

Data shown in Table 1, analyzed in the framework of the minimum three-step mechanism (Scheme 1), indicate that the deacylation step (i.e., k_{+3}; see Scheme 1) is rate-limiting for the cruzain-catalyzed hydrolysis of Z-Arg-Ala-AMC, Z-Phe-Ala-AMC, and Z-Tyr-Ala-AMC (Table 1). It cannot be excluded that instead of the deacylation step, the rate-limiting step may be represented by a conformational change-(s) following product P_2 dissociation and preceding the recovery of the active E species ready for the next catalytic cycle. However, these two catalytic mechanisms are kinetically indistinguishable because the chromophore is represented by the P_1 product. Note that in papain and ficin the rate-limiting step in the hydrolysis of susbstrates displaying Arg or Lys at position P_1 is represented by a conformational change preceding the acylation and deacylation steps (*40*). In this case, kinetics does not fit the minimum three-step catalytic mechanism depicted by Scheme 1.

Binding Energy Calculation for Cruzain/Substrate Recognition. The three-dimensional models of the cruzain:Z-Arg-Ala-AMC, cruzain:Z-Phe-Ala-AMC, and cruzain:Z-Tyr-Ala-AMC noncovalent complexes (i.e., E:S in Scheme 1) are shown in Figure 1, and the calculated energy terms that characterize their formation are given in Table 2.

The total electrostatic free energy opposes binding of Z-Arg-Ala-AMC, Z-Phe-Ala-AMC, and Z-Tyr-Ala-AMC to cruzain. Decomposition of the electrostatic free energy into Coulombic and solvation free energy shows that this is due to the cost of desolvating the polar groups of the protein and substrates upon binding. In fact, in all of the complexes, the ΔG_{sol} value is positive and overcomes the stabilizing

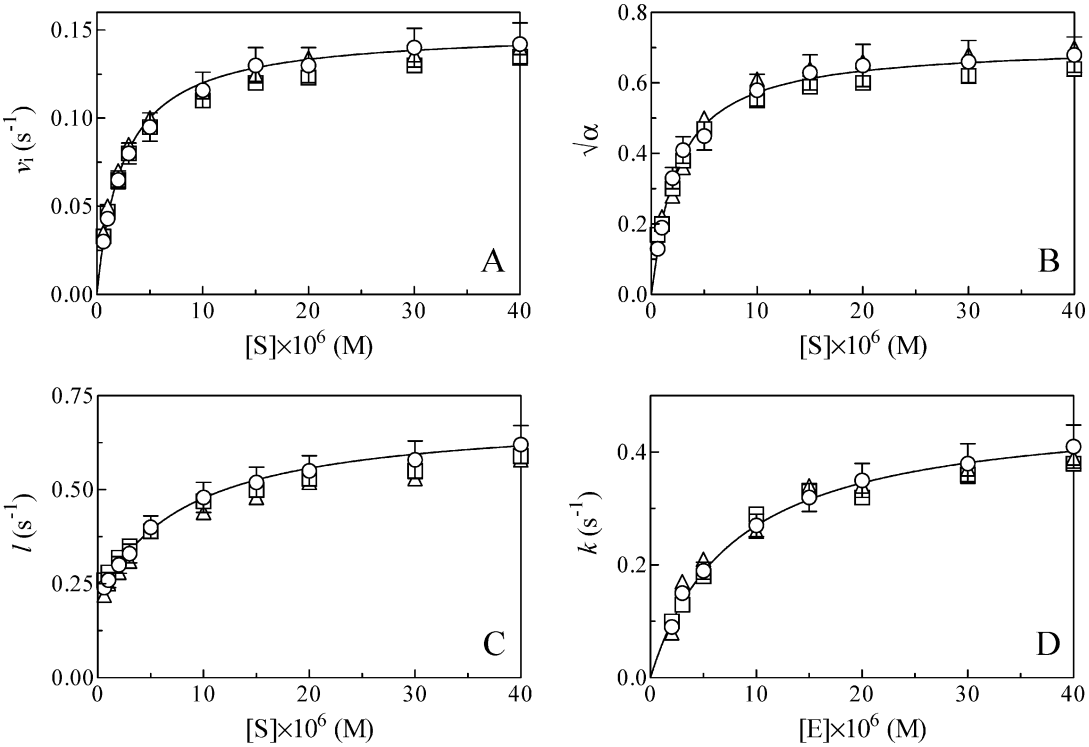

FIGURE 3: Effect of the substrate concentration (i.e., [S]) on the initial velocity (i.e., v_i; A), on the molar fraction of the substrate-bound enzyme (i.e., $\sqrt{\alpha}$; B), and on the first-order rate constant of the burst phase (i.e., l; C) for the cruzain-catalyzed hydrolysis of Z-Arg-Ala-AMC (○), Z-Phe-Ala-AMC (△), and Z-Tyr-Ala-AMC (□), with [S] ≥ 5[E]. Effect of the enzyme concentration (i.e., [E]) on the first-order rate constant of the pre-steady-state reaction (i.e., k; D) for the cruzain-catalyzed hydrolysis of Z-Arg-Ala-AMC (○), Z-Phe-Ala-AMC (△), and Z-Tyr-Ala-AMC (□), with [E] ≥ 5[S]. All data were obtained at pH 6.5 and 37.0 °C. For clarity, only standard deviation and solid lines referring to the cruzain-catalyzed hydrolysis of Z-Arg-Ala-AMC have been reported. The standard deviation is essentially the same for all of the substrates. Solid lines were calculated according to eqs 1 (A), 4 (B), 5 (C), and 6 (D) with values of catalytic parameters given in Table 1. Solid lines were obtained with an iterative nonlinear least-squares curve-fitting procedure. Values of v_i, $\sqrt{\alpha}$, l, and k obtained at different [S] and [E] are significantly different from each other ($p < 0.001$). For further details, see the text.

Table 1: Values of Kinetic Parameters for the Hydrolysis of Z-Arg-Ala-AMC, Z-Phe-Ala-AMC, and Z-Tyr-Ala-AMC Catalyzed by Cruzain (at pH 6.5 and 37.0 °C)

	substrate		
kinetic parameters	Z-Arg-Ala-AMC	Z-Phe-Ala-AMC	Z-Tyr-Ala-AMC
$K_m \times 10^6$ (M)	2.5 ± 0.2^a	2.1 ± 0.2^a	2.1 ± 0.2^a
	2.4 ± 0.2^b	2.3 ± 0.1^b	2.2 ± 0.2^b
k_{cat} (s^{-1})	0.15 ± 0.02^a	0.14 ± 0.02^a	0.13 ± 0.02^a
$(k_{cat}/K_m) \times 10^6$ (M^{-1} s^{-1})	0.060 ± 0.006^a	0.067 ± 0.007^a	0.062 ± 0.007^a
$K_s \times 10^6$ (M)	8.0 ± 0.6^c	7.1 ± 0.6^c	6.8 ± 0.5^c
	7.8 ± 0.6^d	6.9 ± 0.5^d	7.0 ± 0.6^d
k_{+2} (s^{-1})	0.49 ± 0.03^b	0.46 ± 0.03^b	0.45 ± 0.02^b
	0.50 ± 0.03^c	0.45 ± 0.03^c	0.44 ± 0.03^c
	0.48 ± 0.04^d	0.43 ± 0.03^d	0.45 ± 0.03^d
$(k_{+2}/K_s) \times 10^6$ (M^{-1} s^{-1})	0.063 ± 0.006^c	0.063 ± 0.007^c	0.065 ± 0.006^c
	0.062 ± 0.006^d	0.062 ± 0.007^d	0.064 ± 0.006^d
k_{+3} (s^{-1})	0.21 ± 0.02^b	0.18 ± 0.02^b	0.20 ± 0.01^b
	0.20 ± 0.02^c	0.18 ± 0.02^c	0.22 ± 0.02^c
	0.21 ± 0.02^e	0.20 ± 0.03^e	0.18 ± 0.02^e
	0.23 ± 0.02^f	0.19 ± 0.02^f	0.20 ± 0.03^f

[a] Values of K_m, k_{cat}, and k_{cat}/K_m were determined according to eq 1. [b] Values of K_m, k_{+2}, and k_{+3} were determined according to eq 4. [c] Values of K_s, k_{+2}, k_{+2}/K_s, and k_{+3} were determined according to eq 5. [d] Values of K_s, k_{+2}, and k_{+2}/K_s were determined according to eq 6. [e] Values of k_{+3} were calculated according to eq 7. [f] Values of k_{+3} were calculated according to eq 8.

effect of Coulombic interactions. In particular, it is worthwhile to note that the more negative the ΔG_{coul} value is, the more positive the ΔG_{sol} value is, balancing out the two components and yielding very similar ΔG_{el} values for all of the three complexes, irrespective of the polar or nonpolar nature of the P_2 side chain of the substrates considered (Table 2).

As already observed in similar studies (*12*, *31*), the driving force for Z-Arg-Ala-AMC, Z-Phe-Ala-AMC, and Z-Tyr-Ala-AMC binding to cruzain is provided by nonpolar interactions. In all of the three complexes analyzed, more than 60% of the total accessible area of the substrate is buried in the complex resulting in a stabilization ranging approximately from −40 kcal/mol to −50 kcal/mol (Table 2). The higher

Table 2: Comparison between Calculated (ΔG_b) and Experimental (ΔG_{exp}) Binding Free-Energy Values of Cruzain:Z-Arg-Ala-AMC, Cruzain:Z-Phe-Ala-AMC, and Cruzain:Z-Tyr-Ala-AMC Complex Formation[a]

substrate	ΔG_{coul}	ΔG_{solv}	ΔG_{el}	ΔG_{np}	$-T\Delta S_p$	$-T\Delta S_s$	ΔG_b	ΔG_{exp}[b]
Z-Arg-Ala-AMC (A)[c]	−205.5	+222.8	+17.3	−48.2	+5.4	+3.6	−22.0	−7.2
Z-Arg-Ala-AMC (B)[c]	−190.2	+212.1	+21.9	−45.8	+5.4	+3.6	−15.0	
Z-Phe-Ala-AMC	−22.5	+40.1	+17.6	−40.1	+2.0	+1.2	−19.3	−7.3
Z-Tyr-Ala-AMC (A)[c]	−30.0	+55.2	+25.2	−48.6	+3.7	+2.0	−18.0	−7.3
Z-Tyr-Ala-AMC (B)[c]	−30.8	+49.0	+18.2	−49.7	+3.7	+2.5	−25.3	

[a] All energy values are reported in kcal/mol. [b] ΔG_{exp} represents experimentally determined binding energy values calculated from K_s values reported in Table 1. [c] The letters A and B after the substrate name identify the two different conformations of the $ArgP_2$ side chain in the cruzain:Z-Arg-Ala-AMC complex and of the Glu205 side chain for the cruzain:Z-Tyr-Ala-AMC complex. The B conformation of the cruzain:Z-Arg-Ala-AMC complex (40% occupancy) appears to be a crystal-packing artifact in that the $ArgP_2$ side chain is rotated out of the S_2 pocket and forms a salt bridge with the C terminus of another cruzain molecule in the unit cell (*14*). In the B conformation of the cruzain:Z-Tyr-Ala-AMC complex (30% occupancy), Glu205 is rotated away from the inhibitor and fully solvent-exposed (*14*).

Table 3: Values of the Electrostatic Energy (ΔG_{el}) for the Interaction of the Z-Arg-Ala-AMC, Z-Phe-Ala-AMC, and Z-Tyr-Ala-AMC P_2 Side Chains with the Cruzain Glu205 Residue[a]

substrate	ΔG_{coul}[b]	ΔG_{solv}[b]	ΔG_{el}
Z-Arg-Ala-AMC (A)[c]	−35.7	+52.1	+16.4
Z-Arg-Ala-AMC (B)[c]	−22.2	+47.8	+25.6
Z-Phe-Ala-AMC	+15.6	+3.0	+18.6
Z-Tyr-Ala-AMC (A)[c]	+8.4	+11.1	+19.6
Z-Tyr-Ala-AMC (B)[c]	+12.9	+5.3	+18.2

[a] All energy values are reported in kcal/mol. [b] ΔG_{coul} and ΔG_{solv} values have been calculated assigning a charge only to the substrate P_2 side chain and to the Glu205 side chain while keeping the rest of the protein and substrates uncharged. [c] See Table 2.

ΔG_{np} value calculated for the cruzain:Z-Phe-Ala-AMC complex is due to a different conformation of the benzyloxycarbonyl group (Figure 1), which yields a lower contact surface between the enzyme and the substrate. However, the higher ΔG_{np} value in this complex is compensated by a lower entropic penalty because of a higher degree of freedom of the cruzain side chains and benzyloxycarbonyl group itself. In fact, as can be seen from $-T\Delta S_p$ and $-T\Delta S_l$ values (Table 2), restriction of the torsional motion of the substrate and cruzain side chains forming the binding interface accounts for only 3.2 kcal/mol in the cruzain:Z-Phe-Ala-AMC, while the entropic penalty is 6.0 and 9.0 kcal/mol in the cruzain:Z-Tyr-Ala-AMC and cruzain:Z-Arg-Ala-AMC complexes, respectively.

Translational and rotational entropy loss and any strain induced in cruzain and/or in the substrate upon complex formation make a destabilizing contribution to binding. These contributions cannot be calculated directly, even though their magnitude should not exceed 10−15 kcal/mol (*31*), especially in highly rigid systems such as proteases (*12*). Thus, calculated binding free energies are expected to be between 10 and 15 kcal/mol more negative than the experimental ones, as indeed observed (Table 2). This result confirms the reliability of the energy decomposition used in the present study in the analysis of the relative weight of the energetic terms contributing to substrate binding to cruzain.

An interesting result is the substantial similarity of ΔG_{el} values for Z-Arg-Ala-AMC, Z-Phe-Ala-AMC, and Z-Tyr-Ala-AMC binding to cruzain. A deeper analysis of the individual contribution of the interaction between Glu205 and the P_2 residue of the substrates considered (Table 3) reveals that this interaction makes a significant destabilizing contribution to complex formation even when a strong salt bridge is formed between the Arg P2 side chain and Glu205. Interestingly, the interaction between the Phe P2 side chain and Glu205 is only marginally more destabilizing than the one with Arg. This is due to a very low desolvation penalty (3.0 kcal/mol; see Table 3) attributable to the fully solvent-exposed conformation of Glu205 in the cruzain:Z-Phe-Ala-AMC complex. This result represents a further demonstration of the concept that electrostatic interactions, although contributing to the specificity of (macro)molecular recognition, are generally destabilizing from the energetic viewpoint (*12*).

CONCLUSIONS

Present results indicate that the minimum reaction Scheme 1 is operative in cruzain. The catalytic parameters for the cruzain-catalyzed hydrolysis of fluorogenic substrates Z-Arg-Ala-AMC, Z-Phe-Ala-AMC, and Z-Tyr-Ala-AMC showing Arg, Phe, or Tyr at the P_2 position are identical (Table 1). This reflects the ability of the cruzain Glu205 residue to rotate toward the S_2 subsite and interact with the substrate/inhibitor polar P_2 residues (e.g., Arg or Tyr) while being fully solvent-exposed when substrate/inhibitor nonpolar P_2 residues (e.g., Phe) fit the S_2 subsite (see Figure 1 and refs *14*−*16* and *20*).

Theoretical calculations underline the relevant energetic terms determining the low specificity of cruzain. In particular, the mobility of Glu205 allows this residue to minimize the desolvation penalty due to binding of hydrophobic residues in the S_2 subsite of cruzain while maximizing Coulombic interactions when charged residues bind in the S_2 subsite. This is the opposite of what is observed in bovine β-trypsin in which highly specific recognition of substrates and inhibitors is achieved by partial burying of Asp189 on the bottom of the S_1 recognition pocket. This decreases the penalty for desolvation of this residue upon complexation, resulting in a favorable electrostatic contribution of the ion pair formed with the substrate/inhibitor Lys P_1 side chain (*12*). This is not observed in cruzain, in which Glu205 is fully solvent-exposed in the substrate-free enzyme. Thus, when a basic residue binds to the S_2 recognition subsite, the energetic cost of desolvating the two interacting partners is such as to overcome the stabilization due to Coulombic interactions. From this viewpoint, novel inhibitors of cruzain could be designed trying to minimize the desolvation penalty involved in the binding of a basic P_2 residue to the S_2 recognition subsite. This could be achieved by the introduction of a positively charged group in which the charge is

delocalized over a bigger volume, thus increasing the Born radius of the cation and decreasing the energy involved in its desolvation. As an example, cruzain displays a 15-fold decrease in K_m toward the substrate Z-Pya-Arg-AMC (where Pya is L-3-pyridyl-alanine, a positively charged group in which the charge is delocalized over the six-membered ring) as compared to Z-Arg-Arg-AMC (*41*). L-3-Pyridyl-alanine is a weaker base than arginine with an increased hydrophobic character (*41*), but charge desolvation effects likely play a role in such a significant K_m decrease.

The concepts illustrated in the present study are substantiated by the recent characterization of an avirulence protein from the plant pathogen *Pseudomonas syringae*, named AvrPphB, which belongs to a novel family of cysteine proteases (*42*, *43*). In fact, AvrPphB displays a papain-like fold with a deep and positively charged S_2 pocket (*43*), which confers to the enzyme the specificity toward substrates with acidic residues at the P_2 position (*42*). The presence of a solvent-screened Arg residue on the bottom of the AvrPphB S_2 specificity subsite allows selective binding of negatively charged residues minimizing the desolvation penalty, as observed for bovine β-trypsin (*12*).

As final cautions, it must be noted that a failure of the substrates P_2 residue to bind to the S_2 specificity subsite in the initial E:S complex would provide an alternative explanation for the observation of similar catalytic parameters (e.g., K_s values) for the three Z-aminoacyl-aminoacyl-AMC substrates studied. Moreover, more complex catalytic mechanisms could be operative such as the one in which the rate-limiting step of the cruzain catalysis is represented by a conformational change following P_2 product dissociation and preceding the recovery of the active E species ready for the next catalytic cycle.

Last, Z-Arg-Ala, Z-Phe-Ala, and Z-Tyr-Ala derivatives may represent molecular models for the development of "suicide" substrates (i.e., with $k_{+3} \sim 0\ s^{-1}$) of parasitic cysteine proteases that may act as antiparasitic agents. Remarkably, Z-Phe-Ala-FMK stoichiometrically inhibits cruzain and greatly reduces *T. cruzi* parasitemia in a cell-culture system, without adverse effects to mammalian cells (*14*).

ACKNOWLEDGMENT

We thank Dr. Robert J. Fletterick for kindly providing the coordinates of the covalent cruzain·Z-Phe-Ala-FMK adduct and Mr. Angelo Merante for graphical assistance.

REFERENCES

1. Gilles, H. M. (1999) *Protozoal Diseases*, Arnold, London, U.K.
2. McKerrow, J. H., McGrath, M. E., and Engel, J. C. (1995) The cysteine protease of *Trypanosoma cruzi* as a model for antiparasite drug design, *Parasitol. Today 11*, 279−282.
3. Cazzulo, J. J., Stoka, V., and Turk, V. (1997) Cruzipain, the major cysteine proteinase from the protozoan parasite *Trypanosoma cruzi*, *Biol. Chem. 378*, 1−10.
4. McKerrow, J. H., Engel, J. C., and Caffrey, C. R. (1999) Cysteine protease inhibitors as chemotherapy for parasitic infections, *Bioorg. Med. Chem. 7*, 639−644.
5. McKerrow, J. H. (1999) Development of cysteine protease inhibitors as chemotherapy for parasitic diseases: Insights on safety, target validation, and mechanism of action, *Int. J. Parasitol. 29*, 833−837.
6. Ascenzi, P., Salvati, L., Bolognesi, M., Colasanti, M., Polticelli, F., and Venturini, G. (2001) Inhibition of cysteine protease activity by NO-donors, *Curr. Protein Pept. Sci. 2*, 137−153.
7. Colasanti, M., Salvati, L., Venturini, G., Ascenzi, P., and Gradoni, L. (2001) Cysteine protease as a target for nitric oxide in parasitic organisms, *Trends Parasitol. 17*, 575.
8. Cazzulo, J. J. (2002) Proteinases of *Trypanosoma cruzi*: Potential targets for the chemotherapy of Chagas' disease, *Curr. Top. Med. Chem. 2*, 1261−1271.
9. Barrett, A. J., Rawlings, N. D., and Woessner, J. F., Eds. (2004) *Handbook of Proteolytic Enzymes*, 2nd ed., Academic Press, London, U.K.
10. Bode, W., and Huber, R. (1992) Natural protein proteinase inhibitors and their interaction with proteinases, *Eur. J. Biochem. 204*, 433−451.
11. Perona, J. J., and Craik, C. S. (1995) Structural basis of substrate specificity in the serine proteases, *Protein Sci. 4*, 337−360.
12. Polticelli, F., Ascenzi, P., Bolognesi, M., and Honig, B. (1999) Structural determinants of trypsin affinity and specificity for cationic inhibitors, *Protein Sci. 8*, 2621−2629.
13. Ascenzi, P., Bocedi, A., Bolognesi, M., Spallarossa, A., Coletta, M., De Cristofaro, R., and Menegatti E. (2003) The bovine basic pancreatic trypsin inhibitor (Kunitz inhibitor): A milestone protein, *Curr. Protein Pept. Sci. 4*, 231−251.
14. Gillmor, S. A., Craick, C. S., and Fletterick, R. J. (1997) Structural determinants of specificity in the cysteine protease cruzain, *Protein Sci. 6*, 1603−1611.
15. McGrath, M. E., Eakin, A. E., Engel, J. C., McKerrow, J. H., Craik, C. S., and Fletterick, R. J. (1995) The crystal structure of cruzain: A therapeutic target for Chagas' disease, *J. Mol. Biol. 247*, 251−259.
16. Brinen, L. S., Hansell, E., Cheng, J., Roush, W. R., McKerrow, J. H., and Fletterick, R. J. (2000) A target within the target: Probing cruzain's P1′ site to define structural determinants for the Chagas' disease protease, *Struct. Fold Des. 8*, 831−840.
17. Brocklehurst, K., Kowlessur, D., Patel, G., Templeton, W., Quigley, K., Thomas, E. W., Wharton, C. W., Willenbrock, F., and Szawelski, R. J. (1988) Consequences of molecular recognition in the S1−S2 intersubsite region of papain for catalytic-site chemistry. Change in pH-dependence characteristics and generation of an inverse solvent kinetic isotope effect by introduction of a P1−P2 amide bond into a two-protonic-state reactivity probe, *Biochem. J. 250*, 761−772.
18. Patel, M., Kayani, I. S., Templeton, W., Mellor, G. W., Thomas, E. W., and Brocklehurst, K. (1992) Evaluation of hydrogen-bonding and enantiomeric P2−S2 hydrophobic contacts in dynamic aspects of molecular recognition by papain, *Biochem. J. 287*, 881−889. Erratum in (1993) *Biochem. J. 289*, 927.
19. Portaro, F. C., Santos, A. B., Cezari, M. H., Juliano, M. A., Juliano, L., and Carmona, E. (2000) Probing the specificity of cysteine proteinases at subsites remote from the active site: Analysis of P4, P3, P2′, and P3′ variations in extended substrates, *Biochem. J. 347*, 123−129.
20. Huang, L., Brinen, L. S., and Ellman, J. A. (2003) Crystal structures of reversible ketone-based inhibitors of the cysteine protease cruzain, *Bioorg. Med. Chem. 11*, 21−29.
21. Ascenzi, P., Bocedi, A., Visca, P., Antonini, G., and Gradoni, L. (2003) Catalytic properties of cysteine proteinases from *Trypanosoma cruzi* and *Leishmania infantum*: A pre-steady-state and steady-state study, *Biochem. Biophys. Res. Commun. 309*, 659−665.
22. Hollaway, M. R., Antonini, E., and Brunori, M. (1971) The pH-dependence of rates of individual steps in ficin catalysis, *Eur. J. Biochem. 24*, 332−341.
23. Ascenzi, P., Aducci, P., Torroni, A., Amiconi, G., Ballio, A., Menegatti, E., and Guarneri, M. (1987) The pH dependence of pre-steady-state and steady-state kinetics for the papain-catalyzed hydrolysis of *N*-α-carbobenzoxyglycine *p*-nitrophenyl ester, *Biochim. Biophys. Acta 912*, 203−210.
24. Salvati, L., Mattu, M., Polticelli, F., Tiberi, F., Gradoni, L., Venturini, G., Bolognesi, M., and Ascenzi, P. (2001) Modulation of the catalytic activity of cruzipain, the major cysteine proteinase from *Trypanosoma cruzi*, by temperature and pH, *Eur. J. Biochem. 268*, 3253−3258.
25. Mendes, P. (1993) GEPASI: A software package for modelling the dynamics, steady states, and control of biochemical and other systems, *Comput. Appl. Biosci. 9*, 563−571.
26. Mendes, P. (1997) Biochemistry by numbers: Simulation of biochemical pathways with Gepasi 3, *Trends Biochem. Sci. 22*, 361−363.

27. Mendes, P., and Kell, D. B. (1998) Non-linear optimization of biochemical pathways: Applications to metabolic engineering and parameter estimation, *Bioinformatics 14*, 869−883.
28. Brooks, B. R., Bruccoleri, R. E., Olafson, B. D., States, D. J., Swaminathan, S., and Karplus, M. (1983) CHARMM: A program for macromolecular energy minimization and dynamics calculation, *J. Comput. Chem. 4*, 187−217.
29. MacKerell, A. D., Bashford, D., Bellot, M., Dunbrack, R. L., Jr., Field, M. J., Fisher, S., Gao, J., Guo, H., Ha, S., Joseph, D., Kuchnir, L., Kuczera, K., Lau, F. T. K., Mattos, C., Michnick, S., Nguyen, D. T., Ngo, T., Prodom, B., Roux, B., Schlenkrich, M., Smith, J., Stote, R., Straub, J., Wiorkiewicz-Kuczera, J., and Karplus, M. (1992) Self-consistent parametrization of biomolecules for molecular modeling and condensed phase simulation, *Biophys. J. 61*, A143.
30. Huang, L., Brinen, L. S., and Ellman, J. A. (2003) Crystal structures of reversible ketone-based inhibitors of the cysteine protease cruzain, *Bioorg. Med. Chem. 11*, 21−29.
31. Froloff, N., Windemuth, A., and Honig, B. (1997) On the calculation of binding free energies using continuum methods: Application to MHC class I protein−peptide interactions, *Protein Sci. 6*, 1293−1301.
32. Gilson, M. K., and Honig, B. (1988) Calculation of the total electrostatic energy of a macromolecular system: Solvation energies, binding energies, and conformational analysis, *Proteins 4*, 7−18.
33. Smith, K. C., and Honig, B. (1994) Evaluation of the conformational free energy of loops in proteins, *Proteins 18*, 119−132.
34. Nicholls, A., Sharp, K. A., and Honig, B. (1991) Protein folding and association: Insights from the interfacial and thermodynamic properties of hydrocarbons, *Proteins 11*, 281−296.
35. Sitkoff, D., Sharp, K. A., and Honig, B. (1994) Accurate calculation of hydration free energies using macroscopic solvent models, *J. Phys. Chem. 98*, 1978−1988.
36. Sharp, K. A., Nicholls, A., Fine, R. F., and Honig, B. (1991) Reconciling the magnitude of the microscopic and macroscopic hydrophobic effects, *Science 252*, 106−109.
37. Sridharan, S., Nicholls, A., and Honig, B. (1992) A new vertex algorithm to calculate solvent accessible surface areas, *Biophys. J. 61*, A174.
38. Novotny, J., Bruccoleri, R. E., Davis, M., and Sharp, K. A. (1997) Empirical free energy calculations: A blind test and further improvements to the method, *J. Mol. Biol. 268*, 401−411.
39. Pickett, S. P., and Sternberg, M. J. E. (1993) Empirical scale of side-chain conformational entropy in protein folding, *J. Mol. Biol. 231*, 825−839.
40. Hollaway, M. R., and Hardman, M. J. (1973) Evidence for a rate-limiting conformation change in the catalytic steps of the ficin and papain-catalysed hydrolyses of benzyloxycarbonyl-L-lysine *p*-nitrophenyl ester, *Eur. J. Biochem. 32*, 537−546.
41. Alves, L. C., Melo, R. L., Cezari, M. H., Sanderson, S. J., Mottram, J. C., Coombs, G. H., Juliano, L., and Juliano, M. A. (2001) Analysis of the S_2 subsite specificities of the recombinant cysteine proteinases CPB of *Leishmania mexicana*, and cruzain of *Trypanosoma cruzi*, using fluorescent substrates containing non-natural basic amino acids, *Mol. Biochem. Parasitol. 117*, 137−143.
42. Shao, F., Golstein, C., Ade, J., Stoutemyer, M., Dixon, J. E., and Innes, R. W. (2003) Cleavage of *Arabidopsis* PBS1 by a bacterial type III effector, *Science 301*, 1230−1233.
43. Zhu, M., Shao, F., Innes, R. W., Dixon, J. E., and Xu, Z. (2004) The crystal structure of *Pseudomonas* avirulence protein AvrPphB: A papain-like fold with a distinct substrate-binding site, *Proc. Natl. Acad. Sci. U.S.A. 101*, 302−307.

BI048417V